

# **Early Emergence of Anthropogenically-Forced Heat Waves in the Western US and Great Lakes**

Hosmay Lopez<sup>1,2</sup>, Robert West<sup>3</sup>, Shenfu Dong<sup>2</sup>, Gustavo Goni<sup>2</sup>,  
Ben Kirtman<sup>1</sup>, Sang-Ki Lee<sup>2</sup>, and Robert Atlas<sup>2</sup>

<sup>1</sup>Cooperative Institute for Marine and Atmospheric Studies, University of Miami, Miami, Florida

<sup>2</sup>Atlantic Oceanographic and Meteorological Laboratory, NOAA, Miami, Florida

<sup>3</sup>Department of Earth, Ocean and Atmospheric Science, Florida State University, Tallahassee, Florida

*Nature Climate Change*

## Abstract

Climate projections for the 21st Century suggest an increase in the occurrence of heat waves. However, the time at which externally-forced signals of anthropogenic climate change (ACC) emerge against background natural variability (Time of Emergence, ToE) has been challenging to quantify, making future heat wave projections uncertain. Here, we combine observations and model simulations under present and future forcing to assess how internal variability and ACC modulate US heat waves. We show that ACC dominates heat wave occurrence over the Western and Great Lakes regions, with ToE occurring as early as in 2020s 2030s, respectively. In contrast, internal variability governs heat waves in the Northern and Southern Great Plains, where ToE occurs in the 2050s and 2070s; this later ToE is believed to be a result of a projected increase in circulation variability, namely the Great Plain low-level jet. Thus, greater mitigation and adaptation efforts are needed in the Great Lakes and western US regions.

### 1. Introduction

According to the US natural hazard statistics for 2015, extreme heat has been the leading weather-related cause of death in the US for the past 30 years. A few examples of deadly heat waves worldwide include the 1980 heat wave over the Midwest and Southern Plains<sup>1,2</sup> (1,700 fatalities), the 1995 event in Chicago, Illinois<sup>3</sup> (1021 fatalities), the 2003 European heat wave<sup>4</sup> (52,452 fatalities), the 2010 Russian event<sup>5-6</sup> (55,736 fatalities), and the 2011 event over the Great Plains<sup>7</sup> (206 fatalities). Several studies have identified that the effects of anthropogenic climate change (ACC) go beyond simple changes in the mean climate and include changes in the frequency and intensity of extremes<sup>8,9,10</sup> and noted that the number of heat waves and their severity have increased in recent decades<sup>11</sup>. In addition, there will likely be an increased exposure to heat extremes due to population growth<sup>12</sup>. Despite these findings, the impact of ACC

on extreme weather such as heat waves is still not well understood<sup>13-14</sup>. This is especially true for the summer season due to reduced synoptic variability over land<sup>15-16</sup>, where a consensus has not been reached regarding the mechanisms linking extreme events to ACC<sup>17-18-19</sup>. This study reports on the regional dependence and occurrence of heat waves over the US with a focus on future projections and physical mechanisms that may accelerate or slow down the rate of heat extreme occurrence under ACC.

The Fifth Assessment Report of the Intergovernmental Panel on Climate Change (IPCC) evaluated when the signal of ACC will emerge against the background natural variability<sup>20</sup> (i.e., time of emergence or ToE) and found that for surface temperature, the ToE is regional dependent and occurs earlier for the warm season as well as for larger spatial and temporal scales. In contrast, most assessments of regional changes on heat waves associated with ACC are purely based on statistics and the physical mechanisms controlling the ToE for these extreme events have not yet been fully understood. For example, the tails of the surface temperature distributions appear to be sensitive to regional effects and may exhibit non-Gaussian behavior, which may vary regionally, suggesting a need to verify the accuracy of climate models in simulating the distribution tails<sup>21</sup>. Heat waves are linked to specific weather patterns that involve, for example, atmospheric circulation, precipitation deficits, soil moisture content, etc. Atmospheric high-amplitude planetary circulation patterns, such as lingering blocking patterns are also associated with extreme heat wave events<sup>22</sup>.

To arrive at a more reliable projection of heat waves, it is important to describe these extreme events in a physical or phenomenological perspective. To do this, we focus on characterizing heat waves by clustering their spatial distribution and temporal structures. This method allows obtaining the most dominant spatial patterns of extremes whereas more traditional

methods, such as Empirical Orthogonal Functions cannot guarantee the detection of individual dynamical modes due to the non-Gaussian distribution of the extremes<sup>23</sup>. Analyzing ensembles of model results in a purely empirical fashion will suffice for projection and attribution studies but we have to account for the fact that these extremes are present without climate change and natural variability will be a key component in modulating these extremes even under the most pessimistic climate change scenario. Therefore, identification of natural variability, how they may evolve, and their implication on heat waves is essential in assessing the risks of heat related mortality given that natural variability is the main source of uncertainty in future projections.

The rareness of extreme events, the short observational record, and the relative noisiness of mid-latitude atmospheric variability all contribute to making the study of heat waves difficult. To address this challenge, we use the European Center for Mid-Range Weather Forecast (ECMWF) 20th Century Reanalysis<sup>24</sup> (ERA-20C), multiple realizations of the Community Earth System Model (CESM1) Large Ensemble (LE) simulation<sup>25</sup> couple general circulation model, and the Couple Model Intercomparison Project<sup>26</sup> (CMIP5) to examine heat waves in the US, their modulation by internal climate variability versus external forcing, and their non-stationary statistics in a climate change scenario. See supplementary Table 1 for details on models used.

Here, we hypothesize that while internal variability currently dominates the occurrence of heat waves in the US, ACC will gradually assume greater importance as we progress through the 21<sup>st</sup> Century. However, the attribution of heat extremes due to ACC will vary by location. We quantify the time frame for when ACC will dominate the occurrence of heat waves in the 21<sup>st</sup> Century (i.e., ToE).

## 2. Typical heat wave clusters over the United States

A hierarchical clustering algorithm (see methodology section) is applied to daily mean surface temperature from the ERA-20C for the period of 1900-2010. There are eight major regional heat wave clusters identified by the hierarchical algorithm (Fig. 1sm supplementary material). These clusters contain temperature anomalies well above 5°C, affecting large population areas. By definition, clustering of heat waves allows to separate each extreme event from other extremes that are synoptically independent and to investigate these clusters into physically coherent large-scale atmospheric patterns.

Here, we focus on the four heat wave clusters that affect the largest portion of the US population; namely, Western, Northern Plains, Southern Plains, and Great Lakes clusters (Table 1). The spatial structure of these four clusters is shown in Fig. 1. The cluster analysis was also repeated for the 21<sup>st</sup> Century (Supplementary Fig. 2) using the CMIP5 models to test the robustness of these clusters under ACC and also for each of the CMIP5 model used (Supplementary Fig. 3-6). There is a positive trend in the daily mean summer temperature over each cluster region for the 21<sup>st</sup> Century, consistent with the RCP8.5 scenario (Supplementary Fig. 7). There is also an increase in the ratio of warm-to-cold extreme temperature events as shown in Table 1, column 7 (8), for the 20<sup>th</sup> (21<sup>st</sup>) Century. Note that these ratio changes are regionally dependent, with warm extremes becoming significantly more likely for the Great Lakes and Western cluster regions as compared to the Great Plains cluster regions shown in Table 1 (column 9). These changes in the asymmetry of extreme temperature, as well as their regional dependence, may have great implications for future projections of heat waves. It is, therefore, necessary to account not only for changes in the mean but also for changes in the

higher statistical moments (e.g., variance, skewness, and kurtosis) when considering the likelihood of heat wave events<sup>27</sup>.

### 3. Natural variability and its influence on projection uncertainty

The recent apparent pause in warming of the climate system between approximately 1998 and 2014 has led to significant causal debate with respect to natural variability versus changes in external forcing<sup>28-30</sup>, or even whether this pause is an artifact of observational biases<sup>31</sup>. Nevertheless, natural variability plays a key role in masking ACC at regional scales, influencing the occurrence of extreme events and exacerbating the effects of anthropogenic forcing. It is, therefore, necessary to identify the mechanisms that affect the internal variability of heat waves, which is important for future mitigation and planning efforts.

Here, we use the ensemble mean from the CMIP5 and CESM1-LE models as an estimate of the external forcing influence (signal), whereas the ensemble spread quantifies the internal component associated with a particular model ensemble member (noise). It is important to note that the contribution of internal variability to ensemble spread depends on the climate variable, season, and location<sup>32</sup>. The number of heat wave days due to external forcing increases over the US for near-future projections (i.e., 2010-2100) when compared to previous periods for all heat wave clusters (Supplementary Fig. 10). The signal-to-noise ratio (SNR) of heat waves days for the 21<sup>st</sup> Century (i.e., 2020-2100) is significantly smaller for the Great Plains regions (Figs. 1d and 1f) compared to the Great Lakes and Western regions (Figs. 1b and 1h), indicating that future projection of heat waves over the Great Plains is more uncertain due to large natural variability there.

Note that the SNR shown in Fig. 1 is related to the ToE, which is dependent on the uncertainty in the climate response to external forcing and to the amplitude of simulated internal

variability<sup>33</sup>. Future projections show that external forcing will play a more dominant role, especially over the eastern and western thirds of the US; however, the Great Plains region still shows a relatively large influence from internal variability. This is consistent with the concept that at regional scales, internal variability is as important as ACC forcing, at least for the next half century<sup>32,34</sup>.

#### 4. Heat wave response to ACC

Future projections of heat waves are affected not only by changes in the mean temperature but also by changes in the extremes as well. It is, therefore, critical to quantify whether and to what extent non-stationary statistics affect these future projections. To address these issues, a stochastic generated skewed<sup>27</sup> (SGS) probability density function (PDF) of summertime 2m air temperature is quantified for each heat wave cluster depicted in Fig. 1 for the ERA-20C reanalysis, the CESM1-20C and CESM1-21C large ensemble simulations (see Methods). The summers include days from June 1<sup>st</sup> to August 31<sup>st</sup> (i.e., a 92-day summer). Daily mean temperature and a 95<sup>th</sup> percentile threshold is used in the definition of heat waves (see Methods). Fig. 2 shows the SGS for each heat wave region. The CESM1-20C model reproduces the temperature distribution, including the negative skewness, of the ERA-20C reanalysis within all possibilities due to random error and uncertainty due to internal variability (Supplementary Fig. 8), providing confidence in the model. ACC has no significant effect on the asymmetry of the SGS distribution for the Northern (Fig. 2a) and Southern (Fig. 2d) Plains regions. In contrast, the SGS distribution becomes significantly more positively skewed for the heat wave clusters over the Great Lakes (Fig. 2b) and Western (Fig. 2c) regions, suggesting an increase in warm extremes. That is, the frequency of warm extremes is larger for the 21<sup>st</sup> Century and significantly

different (green shading) with respect to the 20<sup>th</sup> Century for the Western and Great Lakes clusters.

The contrasting response of temperature anomalies over these heat wave regions is further investigated by analyzing 1000 realizations of a Markov model for the 20<sup>th</sup> and 21<sup>st</sup> Century CESM1 simulations (see Methods). The increase in the number of warm extremes over the Western and Great Lakes regions (i.e., the ratio of 21°C to 20°C warm extremes of 2.1 and 2.0 respectively, see Table 1) are mostly due to a non-linear (asymmetric) response to changes in the mean and influenced by anthropogenic forcing. In contrast, the modest increase in warm extremes over the two Great Plains regions (i.e., the ratio of 21°C to 20°C warm extremes of 1.6, see Table 1) is dominated by enhanced variability rather than asymmetric changes (Supplementary Fig. 9). These results demonstrate the need for caution in assessing and attributing heat waves due to changes in the mean climate related to ACC forcing as internal variability is large and also impacted by ACC, more notably over the Great Plains.

## 5. Extreme event attribution, internal variability, and ACC

Previous sections indicate the regional dependence of the relative role of internal variability and ACC on the modulation of heat extremes. This motivates the following question: if and/or when ACC become significant with respect to heat extremes? To assess this, we quantify the probability of necessary causality (PN) for all heat extreme events in the 21<sup>st</sup> Century projection (see Methods). The PN of each extreme event is drawn from the generalized Pareto (GP) distribution of summer temperature for each heat wave cluster (Fig. 3). Note that the GP distribution for the 21<sup>st</sup> Century is significantly distinct from that of the 20<sup>th</sup> Century for the Western and Great Lakes heat wave clusters, and the uncertainty due to random error is greatly reduced in the 21<sup>st</sup> Century. In contrast, the 20<sup>th</sup> and 21<sup>st</sup> Century GP distributions for the Great

Plains heat waves (Fig. 3a and 3d) are not statistically well separated for high-threshold extremes (e.g.,  $T > 3.5$  standard deviation).

Figure 4 shows the distribution of PN values for the 21<sup>st</sup> Century projection of heat extremes over each cluster. In general, PN is projected to increase in the future, consistent with the RCP8.5 scenario. More importantly, each cluster has a distinctive evolution of PN. For instance, ACC will be a necessary condition for at least half of the extreme events in a) the Northern Plains after the year  $2056 \pm 2$ , b) the Great Lakes after  $2037 \pm 1$ , c) the Western region after  $2028 \pm 1$ , and d) the Southern Plains not until  $2074 \pm 4$ . These results show that heat extreme attribution to ACC is more certain for the Western and Great Lakes regions. It also demonstrates that internal variability will be the dominant component of Great Plains heat extreme occurrences well past the half-century mark. In fact, it is not until the late 21<sup>st</sup> Century that increased heat waves due to ACC under the RCP8.5 scenario dominate internal variability over the Great Plains. This region also shows a smaller forced-to-internal ratio in the 50-year surface temperature trend<sup>35</sup>.

The attribution or necessary causation analysis shows that in the present climate, the fraction of heat extremes for which ACC plays a dominant role (i.e.,  $PN > 0.5$ ) is still small for all regions. However, the influence of ACC is projected to increase significantly, and  $PN > 0.1$  is already emerging (yellow region in Fig. 4). For the Western region (Fig. 4c), only  $27 \pm 2\%$  of the heat extremes in the 21<sup>st</sup> Century are projected to be entirely due to internal variability, while  $23 \pm 2\%$  are projected to be predominantly caused by ACC. This is in contrast with heat extremes over the Southern Plains (Fig. 4d), where  $62 \pm 4\%$  of extreme heat events are projected to be due to internal variability and only  $8 \pm 4\%$  due to ACC, with a mix of both influences accounting for the remaining 30%.

## 6. Sources of internal variability and uncertainty

Identifying the physical mechanisms that influence the internal variability of heat waves are necessary to improve projections, leading to more oriented mitigation, and adaptation efforts. The atmospheric conditions associated with each heat wave cluster shows a stationary anticyclone pattern located over the extreme warm temperature anomaly (Supplementary Fig. 11). While all four clusters present negative precipitation anomaly patterns, only the two Great Plains clusters depict coherent and large amplitude drier conditions over the actual heat wave region.

There are two potential mechanisms by which changes in the mean climate can modulate the occurrence of extreme temperature events and heat waves. i. Changes in atmospheric circulation as a result of the so-called Arctic amplification<sup>36-37</sup>. ii. Future changes in soil moisture, influencing surface temperature through the land-atmosphere feedback<sup>38-39</sup>. For instance, atmospheric transient eddies (storminess) are strongly negative correlated with surface temperature over the western and northeastern US (Fig. 5a), suggesting that less storminess is linked to warmer surface temperatures. In addition, storm activity over these same regions are projected to decrease significantly for the 21<sup>st</sup> Century (Fig. 5b) due to meridionally asymmetric warming<sup>40</sup>. In contrast, the Great Plains is in a transitional hydrological regime in which soil moisture is a limiting constrain on evapotranspiration and latent heating, influencing climate variability through coupling and feedbacks with the atmosphere<sup>41,42</sup>. Here, more precipitation leads to more soil moisture, decreasing surface air temperature. Also, due to the strong coupling and feedbacks between air temperature and soil moisture, enhanced variability in precipitation and soil moisture will lead to enhanced variability in surface temperature through latent heating, adding uncertainty in future projections of heat extremes.

The question of why the Great Plains events appear to be less sensitive to ACC than those from the Western and Great Lakes clusters is addressed in Fig. 5. The June-July-August (JJA) climatological near surface (925hPa) wind is shown in Fig. 5c for the 20<sup>th</sup> Century CMIP5 ensemble mean depicting a strong southerly flow from the Gulf of Mexico towards the Great Plains knowns as the Great Plains Low Level Jet (GPLLJ). The GPLLJ is responsible for about one third of the total moisture transport into the Great Plains, affecting precipitation<sup>43-46</sup>. The strength of the GPLLJ is positive correlated to moisture transport in the Great Plains (supplementary Figure 12), leading to more precipitation in the Great Plains. In these regions, precipitation is strongly coupled to soil moisture<sup>41</sup>, therefore changes in precipitation associated with the GPLLJ should impact soil moisture and thus surface temperature.

There is currently a positive trend in precipitation over the Great Plains for the spring and summer<sup>47,48</sup>, caused by the strengthening of the GPLLJ<sup>49</sup>. The GPLLJ is also projected to increase in the CMIP5 models (Fig. 5e) as previously found in another study<sup>50</sup>, caused by differential heating between land and adjacent ocean<sup>51</sup>. We also found a strong negative correlation between projected changes in the GPLLJ amplitude and projected changes in the number of heat wave days among CMIP5 models (supplementary Figure 13). This suggests that an enhanced GPLLJ can lead to less heat extremes. On the other hand, the presence of a heat wave in the Great Plains can weaken the GPLLJ due to circulation anomaly as shown in Fig. 5d, but this is beyond the scope of this study. The variability of the GPLLJ is also projected to increase (Fig. 5f), suggesting enhanced uncertainty in future projections of soil moisture and thus surface temperature. Also, an increase in the GPLLJ amplitude should enhance the land-atmosphere feedback as this is a region where soil moisture is a limiting factor for latent heat flux.

In all, the enhanced GPLLJ and moisture transport due to ACC serves to attenuate the anomalous negative (northerly) wind often present during heat wave events which depletes soil moisture. The strong land-atmosphere feedback over the Great Plains along with the projected enhanced variability of the GPLLJ suggests that future projection of heat extremes in the Great Plains is more uncertain and masked by large internal variability (supplementary Fig. 14). It can be said that an enhanced GPLLJ could help alleviate some of the effects of temperature increase due to ACC. This is not the case for the Western and Great Lakes heat wave clusters, where the projected significant reduction of atmospheric transient eddies ensures a robust increase in warm temperature extremes on top of the mean climate shift as shown by the relatively earlier ToE in those regions. Therefore, attributions of heat extremes to ACC in these regions is more certain, as shown by the attribution analysis (Fig. 4). These results hint at the need for caution in attributing heat extremes to changes in the mean given that the relationship of mean climate shifts and their modulation on the higher statistical moments are non-linear and regional in nature. Our study emphasizes that the consequences of increased heat wave amplitude and frequency in the Great Lakes and Western US could be further exacerbated by the large population and rapid population increase in these regions, highlighting the regions where mitigation and adaptation efforts are most required.

**Acknowledgments:** We extend our gratitude to the editor and three anonymous reviewers as their comments have helped improve the manuscript. We would like to acknowledge Drs. David Enfield, Gregory Foltz (NOAA/AOML), Dr. Elizabeth Johns (NOAA/AOML), and Gail Derr (NOAA/AOML) for their comments and suggestions that greatly improved the manuscript. This research was carried out in part under the auspices of the Cooperative Institute for Marine and Atmospheric Studies, a cooperative institute of the University of Miami and the National

Oceanic and Atmospheric Administration (NOAA), cooperative agreement NA10OAR4320143. This work was funded by NOAA's Atlantic Oceanographic and Meteorological Laboratory and by the Climate Observations Division of the NOAA Climate Program Office. SD acknowledge funding by NASA grant NNH13AW33I. HL acknowledges funding from NOAA Climate Program Office its CVP program (GC16-208). S-K.L. acknowledges funding from NOAA Climate Program Office its CVP program (GC16-207). BPK acknowledges funding from the U.S. National Science Foundation (NSF; OCE1419569).

**Contributions:** H.L conceived the study, designed and performed the statistical analysis, and wrote the initial draft of the paper. H.L, R.W, S.D, S.K.L., G.G, B.K., and R.A. contributed to the discussion and interpretation of the results as well as the writing of the final version of the paper.

**Competing financial interests:** The authors declare no competing financial interests.

## References

1. Wolfson, N. & Atlas, R. A simple diagnostic tool for the investigation of persistent phenomena with applications to the summer 1980 U.S. heat wave. *Atmosphere-Ocean* **24**, 111–127 (1986).
2. Meehl, G. A. & Tebaldi, C. More intense, more frequent, and longer lasting heat waves in the 21st century. *Science* **305**, 994–997 (2004).
3. Karl, T. R. & Knight, R. W. The 1995 Chicago heat wave: How likely is a recurrence? *Bull. Am. Meteorol. Soc.* **78**, 107–1119 (1997).

4. Schär, C. Vidale, P. Lüthi, D. Frei, C. Häberli, C. Liniger, M. A. Appenzeller, C. The role of increasing temperature variability in European summer heat waves. *Nature* **427**, 332–336 (2004).
5. Dole, R. *et al.* Was there a basis for anticipating the 2010 Russian heat wave? *Geophys. Res. Lett.* **38**, L06702 (2011).
6. Trenberth, K. E. & Fasullo J. T. Climate extremes and climate change: The Russian heat wave and other climate extremes of 2010. *J. Geophys. Res.* **117**, D17103 (2012).
7. Hoerling, M., and Coauthors. Anatomy of an extreme event. *J. Clim.* **26**, 2811–2832, doi:10.1175/JCLI-D-12-00270.1 (2013).
8. Trenberth KE, Jones PD, Ambenje P, Bojariu R, Easterling D, Klein Tank A, Parker D, Rahimzadeh F, Renwick JA, Rusticucci M, et al., eds. Observations: surface and atmospheric climate change. In: *Climate Change 2007: The Physical Science Basis. Contribution of Working Group I to the Fourth Assessment Report of the Intergovernmental Panel on Climate Change*. Cambridge: Cambridge University Press; 2007.
9. Duffy, P. B. & Tebaldi, C. Increasing prevalence of extreme summer temperatures in the U.S. *Clim. Change* **111**, 487–495 (2012).
10. Kharin, V. V., Zwiers, F. W., Zhang, X. & Wehner, M. Changes in temperature and precipitation extremes in the CMIP5 ensemble. *Clim. Change* **119**, 345–357 (2013).
11. Karl, T. R. & Quayle, R. P. The 1980 summer heat wave and drought in historical perspective. *Mon. Wea. Rev.* **109**, 2055–2073 (1981).

12. Jones, B. O'Neill, B. C. McDaniel, L. McGinnis, S. Mearns, L. O. & Tebaldi, C. Future population exposure to U.S. heat extremes. *Nat. Clim. Change* 5, 652–655, doi:10.1038/nclimate2631 (2015).
13. Kim, O.-Y., B. Wang, and S.-H. Shin (2013), How do weather characteristics change in a warming climate?, *Clim. Dyn.*, 41, 3261–3281, doi:10.1007/s00382-013-1795-8.
14. Cattiaux, J., H. Douville, R. Schoetter, S. Parey, and P. Yiou (2015), Projected increase in diurnal and interdiurnal variations of European summer temperatures, *Geophys. Res. Lett.*, 42, 899–907, doi:10.1002/2014GL062531.
15. Schneider, T., T. Bischoff, and H. Plotka (2014), Physics of changes in synoptic midlatitude temperature variability, *J. Clim.*, doi:10.1175/JCL-D-14-00632.1.
16. Screen, J. A. (2014), Arctic amplification decreases temperature variance in northern mid-to high-latitudes, *Nat. Clim. Change*, 4, 577–582.
17. Palmer, T. N. (2013), Climate extremes and the role of dynamics, *Proc. Natl. Acad. Sci. U.S.A.*, 110, 5281–5282.
18. Shepherd, T. G. (2014), Atmospheric circulation as a source of uncertainty in climate change projections, *Nat. Geosci.*, 7, 703–708.
19. Teng et al. (2016), Projected intensification of subseasonal temperature variability and heat waves in the Great Plains. *GRL*, 43, 2165-2173.
20. Kirtman, B., S.B. Power, J.A. Adedoyin, G.J. Boer, R. Bojariu, I. Camilloni, F.J. Doblas-Reyes, A.M. Fiore, M. Kimoto, G.A. Meehl, M. Prather, A. Sarr, C. Schär, R. Sutton, G.J. van Oldenborgh, G. Vecchi and H.J. Wang, 2013: Near-term Climate Change: Projections and Predictability. In: *Climate Change 2013: The Physical Science Basis. Contribution of Working Group I to the Fifth Assessment Report of the Intergovernmental Panel on*

*Climate Change* [Stocker, T.F., D. Qin, G.-K. Plattner, M. Tignor, S.K. Allen, J. Boschung, A. Nauels, Y. Xia, V. Bex and P.M. Midgley (eds.)]. Cambridge University Press, Cambridge, United Kingdom and New York, NY, USA.

21. Ruff, T. W. & Neelin J. D. Long tails in regional surface temperature probability distributions with implications for extremes under global warming. *Geophys. Res. Lett.* **39**, L04704 (2012).
22. Petoukhov, V., Rahmstorf, S., Petri, S. & Schellnhuber, H. J. Quasiresonant amplification of planetary waves and recent Northern Hemisphere weather extremes. *Proc. Natl. Acad. Sci. USA* **110**, 5336–5341 (2013).
23. Monahan, A. H., Fyfe, J. C., Ambaum, M. H. P., Stephenson, D. B. & North, G. R. Empirical orthogonal functions: The medium is the message. *J. Clim.* **22**, 6501–6514 (2009).
24. Poli, P. *et al.* ERA-20C: An atmospheric reanalysis of the Twentieth Century *J. Clim.* **29**, 4083–4097 (2016).
25. Kay, J. Deser, C. Phillips, A. Mai, A. Hannay, C. Strand, G. Arblaster, The Community Earth System Model (CESM) Large Ensemble Project: A community resource for studying climate change in the presence of internal climate variability. *Bull. Am. Meteorol. Soc.* **96**, 1333–1349 (2015).
26. Taylor, K. E., R. J. Stouffer, and G. A. Meehl, 2012: An overview of CMIP5 and the experiment design. *Bull. Amer. Meteor. Soc.*, 93, 485–498, doi:10.1175/BAMS-D-11-00094.1.
27. Sardeshmukh, D. P., Compo, G. P. & Penland, C. Need for caution in interpreting extreme weather statistics. *J. Clim.* **28**, 9166–9187, doi:10.1175/JCLI-D-15-0020.1 (2015).

28. Tollefson, J. The case of the missing heat. *Nature* **505**, 276–278, doi:10.1038/505276a (2014).
29. Solomon, S. Daniel, J. S., Neely, R. R., Vernier, J. P., Dutton, E. G., & Thomason, L. W. The persistently variable “background” stratospheric aerosol layer and global climate change. *Science* **333**, 866–870 (2011).
30. Clement, A. & DiNezio, P. The tropical Pacific Ocean—Back in the driver's seat? *Science* **343**, 976–978 (2014).
31. Karl, T. R. *et al.* Possible artifacts of data biases in the recent global surface warming hiatus. *Science* **348**, 1469–1472 (2015).
32. Deser, C., Knutti, R., Solomon, S. & Phillips, A. S. Communication of the role of natural variability in future North American climate. *Nat. Clim. Change*, **2**, 775–779, doi:10.1038/nclimate1562 (2012a).
33. Hawkins E. & Sutton R. Time of emergence of climate signals. *Geophys. Res. Lett.* **39**, l01702 (2012).
34. Wallace, J. M., Deser, C., Smoliak, B. V. & Phillips, A. S. Attribution of climate change in the presence of internal variability. *Climate Change: Multidecadal and Beyond. In World Scientific Series on Asia-Pacific Weather and Climate Vol 6* (2013)
35. Deser, C., Phillips, A. S., Alexander, M. A. & Smoliak, B. V. Projecting North American Climate over the next 50 years: Uncertainty due to internal variability. *J. Clim.* **27**, 2271–2296 (2014).
36. Barnes, E. A., and J. A. Screen (2015), The impact of Arctic warming on the midlatitude jetstream: Can it? Has it? Will it?, *WIREs Clim. Change*, **6**, 277–286.

37. Coumou, D., J. Lehmann, and J. Beckmann (2015), The weakening summer circulation in the Northern Hemisphere mid-latitude, *Science*, 348, 324–327.

38. Koster, R. D., et al. (2004), Regions of strong coupling between soil moisture and precipitation, *Science*, 305, 1138–1140.

39. Fischer, E. M., J. Rajczak, and C. Schär (2012), Changes in European summer temperature variability revisited, *Geophys. Res. Lett.*, 39, K19702, doi:10.1029/2012GL052730.

40. Lehmann, J., D. Coumou, K. Frieler, V. Eliseev, and A. Livermann (2014), Future changes in extratropical storm tracks and baroclinicity under climate change, *Environ. Res. Lett.* 9, 084002.

41. Koster, R.D., Guo, Z.C., Dirmeyer, P.A., Bonan, G., Chan, E., Cox, P., Davies, H., Gordon, C.T., Kanae, S., Kowalczyk, E., Lawrence, D., Liu, P., Lu, C.H., Malyshev, S., McAvaney, B., Mitchell, K., Mocko, D., Oki, T., Oleson, K.W., Pitman, A., Sud, Y.C., Taylor, C.M., Verseghy, D., Vasic, R., Xue, Y.K., Yamada, T. GLACE: The Global Land–Atmosphere Coupling Experiment. Part I: overview. *J. Hydrometeorol.* 7, 590–610 (2006).

42. Seneviratne SI, Corti T, Davin EL, Hirschi M, Jaeger EB, Lehner I, Orlowsky B, Teuling AJ. Investigating soil moisture–climate interactions in a changing climate: A review. *Earth-Science Reviews*. May 31;99(3):125-61 (2010).

43. Walters, C. K. & Winkler, J. A. Airflow configurations of warm season southerly low-level wind maxima in the Great Plains. Part I: Spatial and temporal characteristics and relationship to convection. *Wea. Forecasting* 16, 513–530 (2001).

44. Wexler, H. A boundary layer interpretation of the low level jet. *Tellus* 13, 368–378 (1961).

45. Jiang, X., Lau, N.-C., Held, I. M. & Ploshay, J. J. Mechanisms of the Great Plains low-level jet as simulated in an AGCM. *J. Atmos. Sci.* 64, 532–547 (2007).

46. Cook, K. H., Vizy, E. K., Launer, Z. S. & Patricola, C. M. Springtime intensification of the Great Plains low-level jet and Midwest precipitation in GCM simulations of the twenty-first century. *J. Clim.* 21, 6321–6384 (2008).
47. Kunkel, K. E. et al. Monitoring and understanding trends in extreme storms: state of knowledge. *Bull. Am. Meteor. Soc.* 94, 499–514 (2013).
48. Janssen, E., Wuebbles, D. J., Kunkel, K. E., Olsen, S. C. & Goodman, A. Observational- and model-based trends and projections of extreme precipitation over the contiguous United States. *Earth's Future* 2, 99–113 (2014).
49. Feng, Z., Leung, L. R., Hagos, S., Houze, R. A., Burleyson, C. D., & Balaguru, K. More frequent intense and long-lived storms dominate the springtime trend in central US rainfall. *Nature Communications*, 7, 13429 (2016).
50. Tang, Y., J. Winkler, S. Zhong, X. Bian, D. Doubler, L. Yu, C. Walters. Future changes in the climatology of the Great Plains low-level jet derived from fine resolution multimodel simulations, *Scientific reports*, 7, 5029. Doi:10.1038/s41598-017-05135-0 (2017).
51. Cook, K. H., Vizy, E. K., Launer, Z. S. & Patricola, C. M. Springtime intensification of the great plains low-level jet and midwest precipitation in GCM simulations of the twenty-first century. *J. Climate* 21, 6321–6340 (2008).

## Methods

### Models and observational datasets

The ERA-20C reanalysis is used as an estimate of historical heat wave occurrence over the US and to assess the fidelity of the CESM1-LE and the CMIP5 models in reproducing the spatial patterns of heat waves. A multi-century pre-industrial run from CESM1-LE is used to quantify heat wave statistics in the absence of anthropogenic forcing. CESM1-LE and CMIP5 model simulations under 20<sup>th</sup> Century and Representative Carbon Path future scenario (RCP8.5) are analyzed for heat waves under external forcing. The CESM1-LE simulation provides a large ensemble size from a single model; consequently, the ensemble spread is solely due to internal climate variability<sup>25</sup>, whereas the CMIP5 simulations provide a multi-model ensemble approach aimed at reducing model errors by ensemble averaging. We analyzed a 1000-year pre-industrial simulation (CESM1-PI) with constant 1850 forcing as the basis for the internal variability of heat waves, a 30-member ensemble simulation (CESM1-LE) for the period of 1920-2100, and multiple CMIP5 models for the period of 1920-2100. Each model simulation has a distinct climate trajectory due to differences in the atmospheric initial conditions. All models have the same specified external forcing, with historical forcing from 1920-2005 and Representative Carbon Path 8.5 forcing<sup>52-53</sup> from 2006 to 2100 following CMIP5 design protocol.

### Heat wave cluster

The definition of heat wave proposed here is based on clustering of the daily mean temperature that covers each summer from 1 June to 30 August<sup>54</sup>. For a temperature extreme to qualify as a heat wave, it must satisfy the following three constraints:

- a) Threshold anomaly: For each day and grid point, a temperature anomaly with respect to the daily mean climatology is defined. The daily mean climatology is smoothed with a 20-day

running average. The 20-day smoothing of the daily climatology is performed to account for the synoptic variability of typical extreme heat anomalies. Extremes are defined as anomalies larger than the 95<sup>th</sup> percentile threshold.

- b) *Spatial smoothing*: A spatial filter is applied to the threshold anomalies to eliminate the influence of small-scale extremes (i.e., hot grid points). Each grid point is used as the center of a square of size  $L$ . A sliding scan is performed, and only those points for which the fraction of threshold anomalies exceeds some ratio  $\alpha$  are retained. It should be noted that the number of grid points (i.e., stations) within the  $L^2$  region depends on the resolution of the temperature data.  $L$  was chosen so that the sliding scan has a horizontal resolution of about 4° in latitude and longitude. We tested the sensitivity of this parameter ranging from 2° <  $L$  < 6° without much change in the distribution of the clusters nor in the dissimilarity index.
- c) *Temporal smoothing*: The criteria for a) and b) must be met for a minimum of 3 consecutive days to exclude short-duration events, which are uncharacteristic of synoptic and planetary scale heat waves. Propagating events are accounted for by merging events with overlapping areas of more than 40% during the 3-day window.

Events that satisfied the above three constraints were considered to be heat wave events. These events were clustered using a hierarchical clustering algorithm<sup>54-56</sup>, which was previously applied to European heat waves<sup>54</sup>. The clustering algorithm comprises the following three steps:

- d) For each event map, temperature anomalies that did not satisfy the previous three constraints are set to zero, and those that did satisfy the three constraints are retained. In the case of heat waves, all anomalies are positive by definition.

- e) All maps belonging to a specific event are merged into a single event. That is, a single heat wave event includes several daily temperature anomaly maps that are averaged into a single heat wave. Therefore, each heat wave event is an independent cluster.
- f) The agglomerative hierarchical clustering algorithm is applied to the clusters defined in step (e). The algorithm quantifies the inter-cluster distance between two clusters  $M$  and  $N$  using equation (1). The two closest clusters are merged into a single new cluster. This procedure is repeated until a stop criterion is met, which sets the final number of clusters.

$$d(M, N) = 1 - \frac{\sum_{i=1}^I \sum_{j=1}^J M_{i,j} N_{i,j}}{\left[ \sum_{i=1}^I \sum_{j=1}^J M_{i,j}^2 \right]^{\frac{1}{2}} \left[ \sum_{i=1}^I \sum_{j=1}^J N_{i,j}^2 \right]^{\frac{1}{2}}} = 1 - r(M, N(1)) \quad (1)$$

Here,  $r(M, N)$  is the spatial correlation of clusters  $M$  and  $N$  over all grid points  $I$  and  $J$ . The inter-cluster distance is taken as the average distance between all members of clusters  $M$  and  $N$ . The dissimilarity index (1) provided the optimum number of clusters, which was found to be 8 clusters.

### Stochastic Generated Skewed PDF

For each heat wave cluster, we assess changes in the PDF of summer temperature extremes by modeling the PDF as a stochastically generated skewed (SGS) distribution<sup>27</sup>. The SGS of a variable  $X$  is defined in equation (2), where  $E$ ,  $g$ ,  $b$ , and  $N$  are parameters obtained from the statistical moments of  $X$ .

$$SGS(X) = \frac{1}{N} [(EX + g)^2 + b^2]^{-\left[1 + \left(\frac{1}{E^2}\right)\right]} \exp \left[ \frac{2g}{E^2 b} \tan^{-1} \left( \frac{EX + g}{b} \right) \right] \quad (2)$$

A Markov model<sup>27</sup> for the variable  $X_i$  is defined in equation (3) using the same parameters as the SGS distribution. Note that the model is damped and forced by cumulative additive ( $b\eta_1 + g\eta_2$ ) and multiplicative ( $EX_i\eta_2$ ) noise, where  $\eta_1$  and  $\eta_2$  are random Gaussian variables with a zero mean and unit variance. Equation (3) is integrated forward using a fourth order Runge-Kutta method, with a time step ( $dt = 1$  hour) and decorrelation time scale ( $\lambda = 4$  days) to produce 81 summers of 92-day length. This process is repeated 1000 times for a total of 1000 time series of 7452-day length, which is the same length of the 1920-2000 and 2020-2100 summer periods for the 20<sup>th</sup> and 21<sup>st</sup> centuries used here.

$$X_{i+1} = X_i - \left[ \left( 1 + \frac{E^2}{2} \right) X_i + \frac{Eg}{2} \right] \lambda dt + [b\eta_1 + (EX_i + g)\eta_2] \sqrt{\lambda dt} \quad (3)$$

This approach allows us to quantify the non-Gaussian aspect of the meteorological fields (e.g., surface temperature for our purpose). The modeling of 2 m temperatures using the SGS approach brings several main benefits. First, it provides a means to quantify the influence of climate shifts under Gaussian and non-Gaussian assumptions. Second, it enables us to investigate how changes in climate influence the statistical moments of summer temperature and its PDF. Lastly, the parameters of the SGS distribution can be used to define the shape and scale parameters of the extreme value generalized Pareto (GP) distribution<sup>27</sup>. The Markov model is also used to assess confidence interval for the GP distribution due to random errors.

## Probability of necessary causation (PN)

Here, PN is the fraction of extreme events attributed to ACC, defined as:

$$PN = \max \left\{ 1 - \frac{P_0}{P_1}, 0 \right\} \quad (4)$$

where  $P_0$  is the probability of an event occurring in the counter-factual world (i.e., without ACC) and  $P_1$  is the probability of that same event occurring in the factual world (i.e., including ACC).  $PN$  ranges from zero to one and indicates whether ACC is a necessary condition for the extreme event to occur. That is, the extreme event would not occur in the absence of ACC. The probabilities  $P_0$  and  $P_1$  are obtained from a GP distribution of the pre-industrial and 21<sup>st</sup> Century summer temperatures, respectively.

Given that extreme events are by definition rare,  $PN$  is quantified using all heat extremes in all 30 ensembles of the 21<sup>st</sup> Century run. Then, for each decade, all  $PN$  values are binned into three groups;  $PN \leq 0.1$  (ACC is not a necessary condition for most heat extremes),  $0.1 < PN \leq 0.5$ , and  $PN > 0.5$  (ACC is a necessary condition for more than half of the temperature extremes). For example, a distribution of  $PN$  spanning the summers of 2010-2019 and all 30 ensembles for a total of 300 summers is quantified. This is repeated for all decades, which allows for a representative sample size of heat extremes. The results are presented in Fig. 4 as a probability plot of  $PN$  values for each decade and bin. This allows us to make assessments of heat extreme attribution to ACC into the future.

## Transient eddies (storminess) definition

Transient eddies are defined as the square of the departure from the monthly mean of daily mean geopotential height at 500hPa.

**Data availability.** The data that support the findings of this study are available from the corresponding author upon request.

## References for methods

52. Meinhausen, M. & Coauthors. The RCP greenhouse gas concentration and their extension from 1765 to 2300. *Clim. Change* **109**, 213, doi:10.1007/s10584-011-0156-z (2011).
53. Lamarque, J. F. & Coauthors. Global and regional evolution of short-lived radiatively-active gases and aerosols in the Representative Concentration Pathways. *Clim. Change.*, **109**, 191–212 (2011).
54. Stefanon, M., Fabio, D. & Drobinski, P. Heat wave classification over Europe and the Mediterranean region. *Environ. Res. Lett.* **7**, 014023 (2012).
55. Smyth, P., Ide, K. & Ghil, M. Multiple regimes in Northern Hemisphere height fields via mixture model clustering. *J. Atmos. Sci.* **56**, 3704–3723 (1999).
56. Tan, P. N., Steinbach, M. & Kumar, V. *Introduction to Data Mining* (Reading, MA, Addison-Wesley) 769 p. (2006).

## Tables and figures captions

**Table 1. Statistics of summer 2m air temperature extremes for the 20<sup>th</sup> Century (20C) and 21<sup>st</sup> Century (21C) projections.** Return periods are shown for the 20C, 21C, 20C plus mean changes (i.e., shape preserving distribution with no variance or higher moment changes), and 21C with no mean shift PDF (i.e., return period due solely to variance and higher moment

changes). Uncertainty intervals denoted by a plus/minus sign correspond to the 99% confidence interval based on all 1000 realizations of a Markov model. The eight-digit number under each cluster name indicates the population count affected by the cluster.

**Figure 1. Geographic distribution of heat waves.** a) 20<sup>th</sup> Century 2m temperature anomaly and b) 21<sup>st</sup> Century PDF of the signal-to-noise ratio (SNR) of heat wave events for the Great Lakes cluster. Similarly, c) and d) for the Northern Plains, e) and f) Southern Plains, and g) and h) Western heat wave clusters from the ensemble mean of CMIP5 models. The SNR PDF is obtained by randomly selecting eight models (ensembles) 1000 times from the CMIP5 (CESM1-LE) simulations. The mean SNR is shown in black and 95% confidence interval in red (blue) from the CMIP5 (CESM-LE). The 20<sup>th</sup> Century SNR is shown by green diamond.

**Figure 2. Stochastic generated skewed (SGS) PDF of summertime 2m temperature anomalies,** a) Northern Plains, b) Great Lakes, c) Western, and d) Southern Plains regions. The ERA-20C reanalysis for the 1920-2000 period is shown by the black line, the CESM1-20C (1920-2000) is shown as blue line, and the CESM1-21C (2020-2100) is depicted by the red line. The spread depicted by lighter colors represents the 99% confidence interval using all 1000 realizations of the Markov model, providing uncertainty due to random error. The green shading indicates statistically-significant differences between the 20C and 21C PDF at a 99% confidence level.

**Figure 3. Generalized Pareto (GP) distribution for the daily mean JJA standardized temperature anomalies for the 20<sup>th</sup> (blue) and 21<sup>st</sup> Century (red) curve,** a) Northern Plains, b) Great Lakes, c) Western, and d) Southern Plains regions. The standard anomaly is derived by dividing the daily anomaly by the respective daily standard deviation. A standard anomaly is

chosen for an easier comparison among regions (panels). Vertical bars indicate the 99% range of uncertainty based on all 1000 realizations of the Markov model.

**Figure 4. Probability of necessary causation (PN) of heat waves,** a) Northern Plains, b) Great Lakes, c) Western, and d) Southern Plains regions. PN values are binned into: PN  $\leq 0.1$  (blue region, e.g., ACC is not a necessary condition for heat waves),  $0.1 < PN \leq 0.5$  (yellow, ACC is somewhat important) and  $PN > 0.5$  (red, ACC is a necessary condition for heat waves). The intersection of the dashed lines denotes when ACC becomes a major contributor to heat extremes (e.g., a measure of the time of emergence). The percentage values indicate the fraction of heat extremes attributed to each category. The plus/minus value and the gray shading indicates 95% confidence interval by randomly selecting 20 ensemble members 500 times.

**Figure 5. Great Plains Low Level Jet and heat waves.** a) Regression of JJA transient eddies and 2m temperature [ $\text{hPa}^2/\text{^{\circ}C}$ ]. b) Projected changes of JJA transient eddies [ $\text{hPa}^2$ ]. c) CMIP5 ensemble mean JJA 925hPa wind (vector) and meridional wind (color) from the historical period. d) Same as c) but the composite during Northern and Southern Great Plains heat waves from the historical period. e) Same as c) but 21<sup>st</sup> minus 20<sup>th</sup> Century JJA 925hPa winds. f) Variance ratio of 21<sup>st</sup> to 20<sup>th</sup> Century JJA 925hPa meridional wind. Stipples in a-d) and f) indicate 95% level based on a Student-T test and F-test respectively.

**Table 1.** Changes in the mean, return period, and ratio of extreme warm and cold events of magnitude greater than  $3\sigma$  (standard deviations) for the summer 2-m air temperature of the four cluster regions for 20<sup>th</sup> Century (20°C) and 21<sup>st</sup> Century (21°C) projections. Return periods are shown for the 20°C, 21°C, 20°C plus mean changes (i.e., shape preserving distribution with no variance or higher moment changes), and 21°C with no mean shift PDF (i.e., return period due solely to variance and higher moment changes). Uncertainty intervals denoted by a plus/minus sign correspond to the 99% confidence interval based on all 1000 realizations of a Markov model. The eight-digit number under each cluster name indicates the population count affected by the cluster.

		Return Period (years) of events $> 3\sigma$				Ratios of events $> 3\sigma$		
Cluster (Population)	Mean 20°C (21°C)	20°C PDF	21°C PDF	20°C PDF plus mean shift	21°C PDF with no mean shift	Ratio of 20°C warm to 20°C cold	Ratio of 21°C warm to 21°C cold	Ratio 21°C warm to 20°C warm
West (63,160,900)	23.2 $\pm$ 0.7 (27.5 $\pm$ 0.8)	<b>376 <math>\pm</math> 3</b>	<b>17 <math>\pm</math> 14</b>	<b>60 <math>\pm</math> 7</b>	<b>67 <math>\pm</math> 6</b>	<b>0.6 <math>\pm</math> 0.1</b>	<b>6.4 <math>\pm</math> 0.6</b>	<b>2.1 <math>\pm</math> 0.1</b>
Northern Plains (46,843,000)	21.7 $\pm$ 0.4 (26.3 $\pm$ 0.7)	<b>410 <math>\pm</math> 3</b>	<b>17 <math>\pm</math> 14</b>	<b>55 <math>\pm</math> 7</b>	<b>65 <math>\pm</math> 6</b>	<b>0.6 <math>\pm</math> 0.1</b>	<b>1.7 <math>\pm</math> 0.2</b>	<b>1.6 <math>\pm</math> 0.1</b>
Southern Plains (37,900,200)	23.4 $\pm$ 0.4 (27.4 $\pm$ 0.6)	<b>404 <math>\pm</math> 3</b>	<b>21 <math>\pm</math> 12</b>	<b>68 <math>\pm</math> 6</b>	<b>73 <math>\pm</math> 6</b>	<b>0.7 <math>\pm</math> 0.1</b>	<b>1.7 <math>\pm</math> 0.2</b>	<b>1.6 <math>\pm</math> 0.1</b>
Great Lakes (78,935,400)	16.5 $\pm$ 0.4 (20.6 $\pm$ 0.6)	<b>364 <math>\pm</math> 3</b>	<b>20 <math>\pm</math> 13</b>	<b>61 <math>\pm</math> 7</b>	<b>70 <math>\pm</math> 6</b>	<b>0.6 <math>\pm</math> 0.1</b>	<b>10.2 <math>\pm</math> 1.2</b>	<b>2.0 <math>\pm</math> 0.1</b>

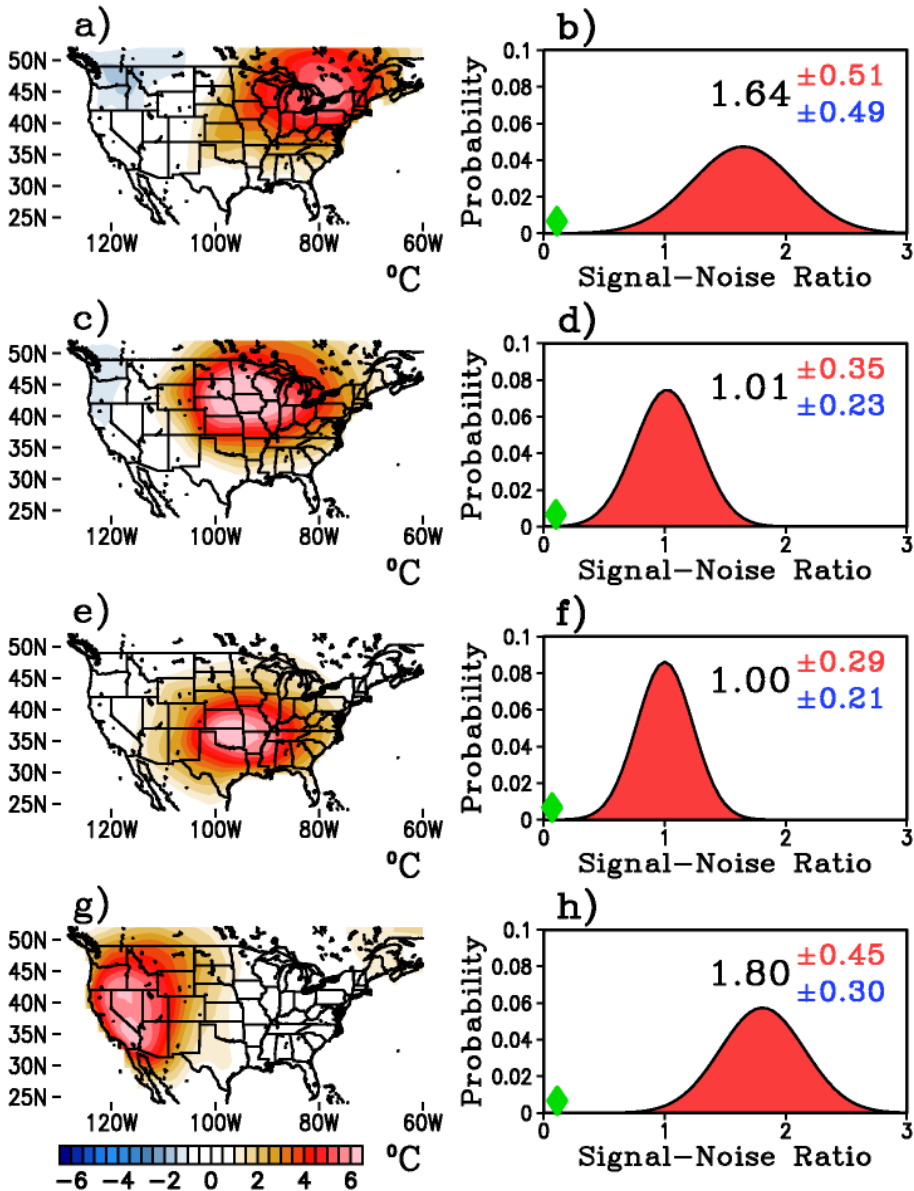


**Figure 1.** 20<sup>th</sup> Century 2-m air temperature anomaly associated with; a) Great Lakes, c) Northern Plains, e) Southern Plains, and g) Western heat wave cluster from the ensemble mean of the CMIP5 models. The 21<sup>st</sup> Century PDF of the signal-to-noise ratio (SNR) of heat wave events over the; b) Great Lakes, d) Northern Plains, f) Southern Plains, and h) Western cluster region. The signal (noise) is defined as the ensemble mean (spread) of the number of heat wave events. To obtain the PDF of SNR, eight models (ensemble members) from the CMIP5 (CESM1-LE) simulations are randomly selected and the SNR is computed separately for the CMIP5 and the CESM1-LE. This is repeated a 1000 time. The mean SNR is shown in black and the 95% confidence interval is depicted in red from the CMIP5, which includes internal variability and model error, and blue from the CESM-LE, which includes internal variability alone. The 20<sup>th</sup> Century SNR is shown by the green diamond.

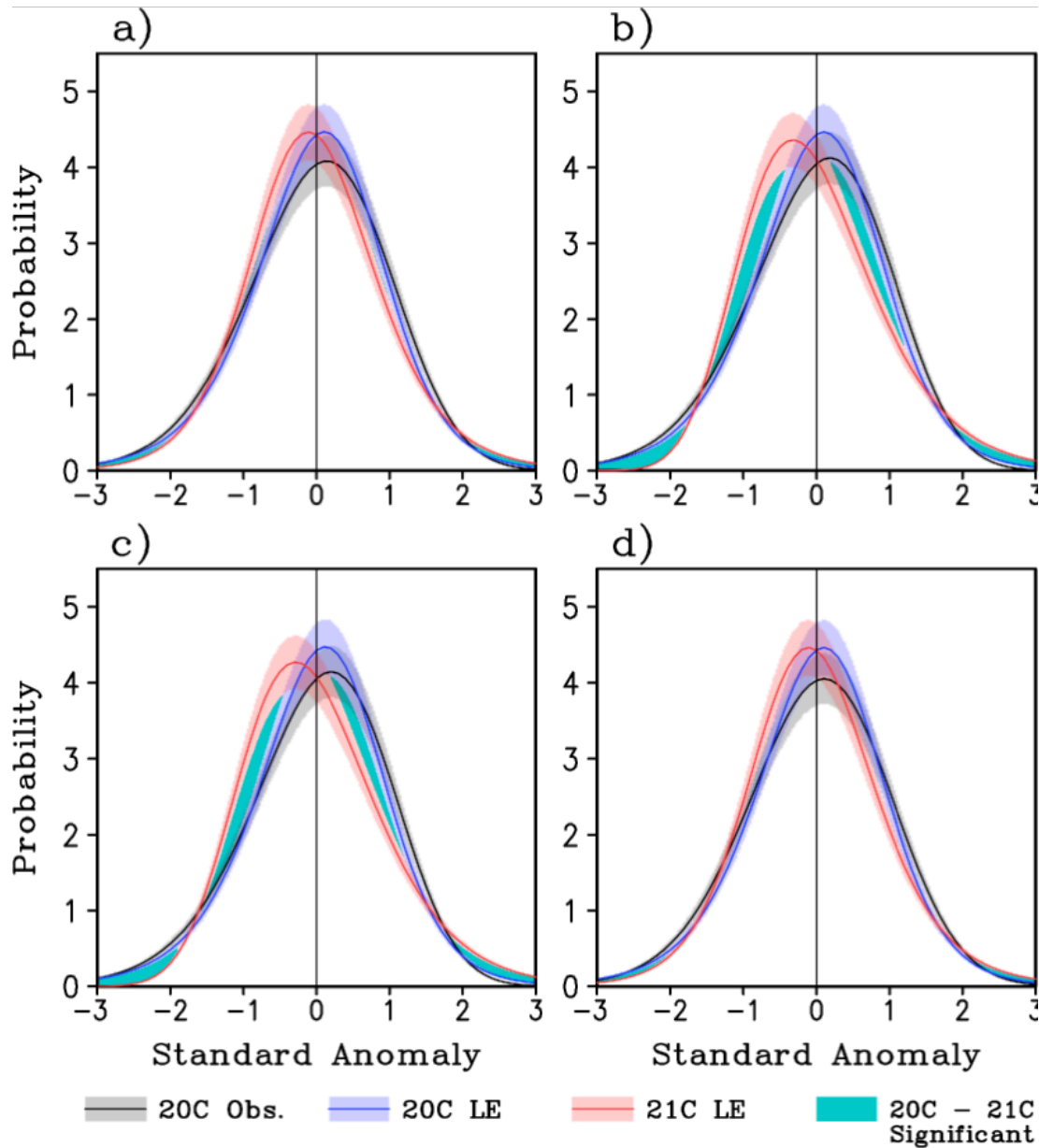


**Figure 2.** Stochastic generated skewed (SGS) probability density function (PDF) of summertime 2-m air temperatures for the a) Northern Plains, b) Great Lakes, c) Western, and d) Southern Plains regions. The ERA-20C reanalysis for the 1920-2000 period is shown as a black contour, the CESM1-20C (1920-2000) simulation is shown as a blue contour, and the CESM1-21C (2020-2100) simulation is depicted as a red contour. The spread depicted by the lighter color for each curve represents the 99% confidence interval based on all 1000 realizations of a Markov model. This spread provides for uncertainty due to random error. The light-blue shading indicates statistically-significant differences between the 20°C and 21°C PDF at a 99% confidence level. All temperature anomalies were normalized by their standard deviation.

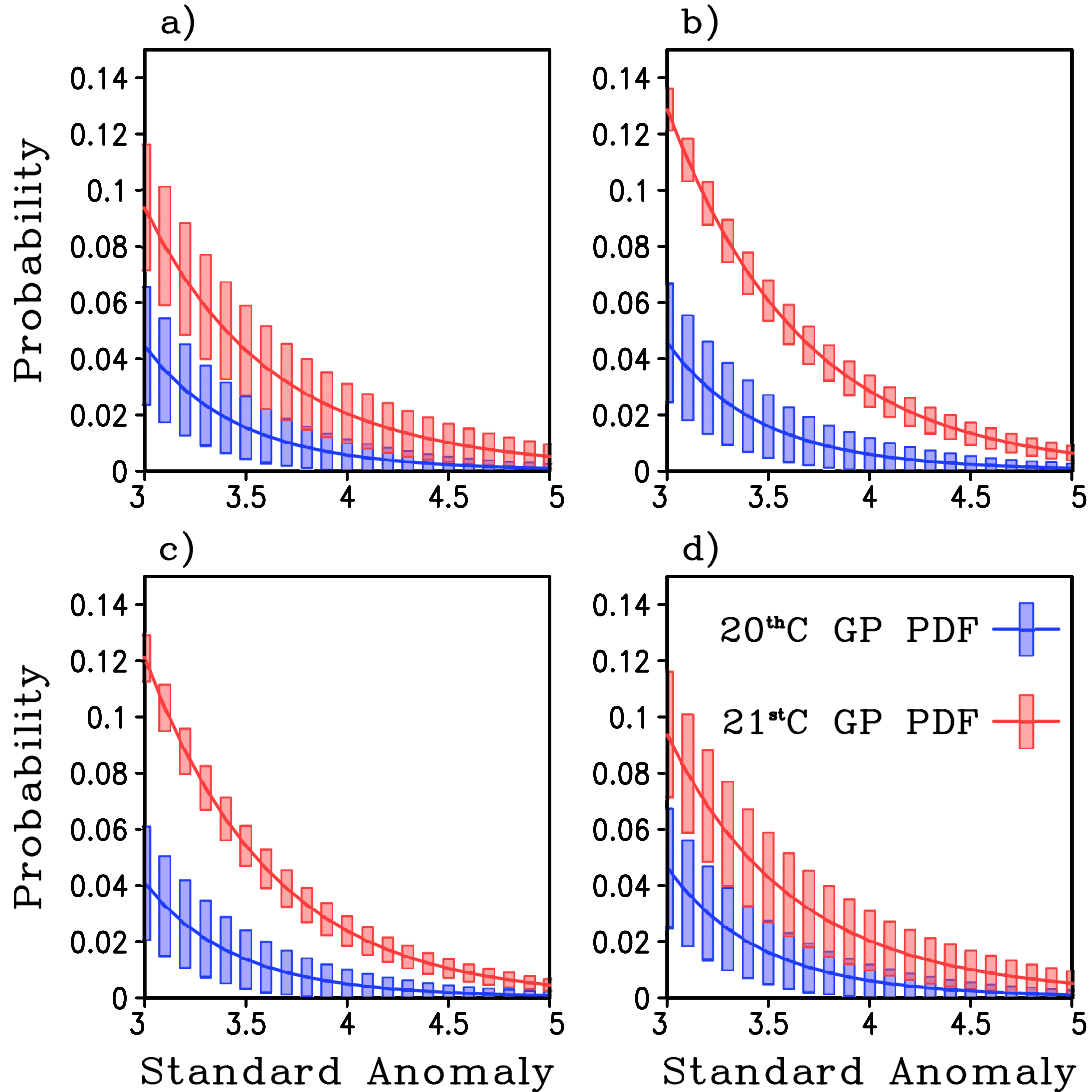


**Figure 3.** Generalized Pareto (GP) distribution for the daily mean JJA standardized temperature for the a) Northern Plains, b) Great Lakes, c) Western, and d) Southern Plains regions from the CESM1-LE. The standard anomaly is derived by dividing the daily anomaly by the respective daily standard deviation. A standard anomaly is chosen for an easier comparison among regions (panels). Vertical bars indicate the 99% range of uncertainty based on all 1000 realizations of the Markov model.

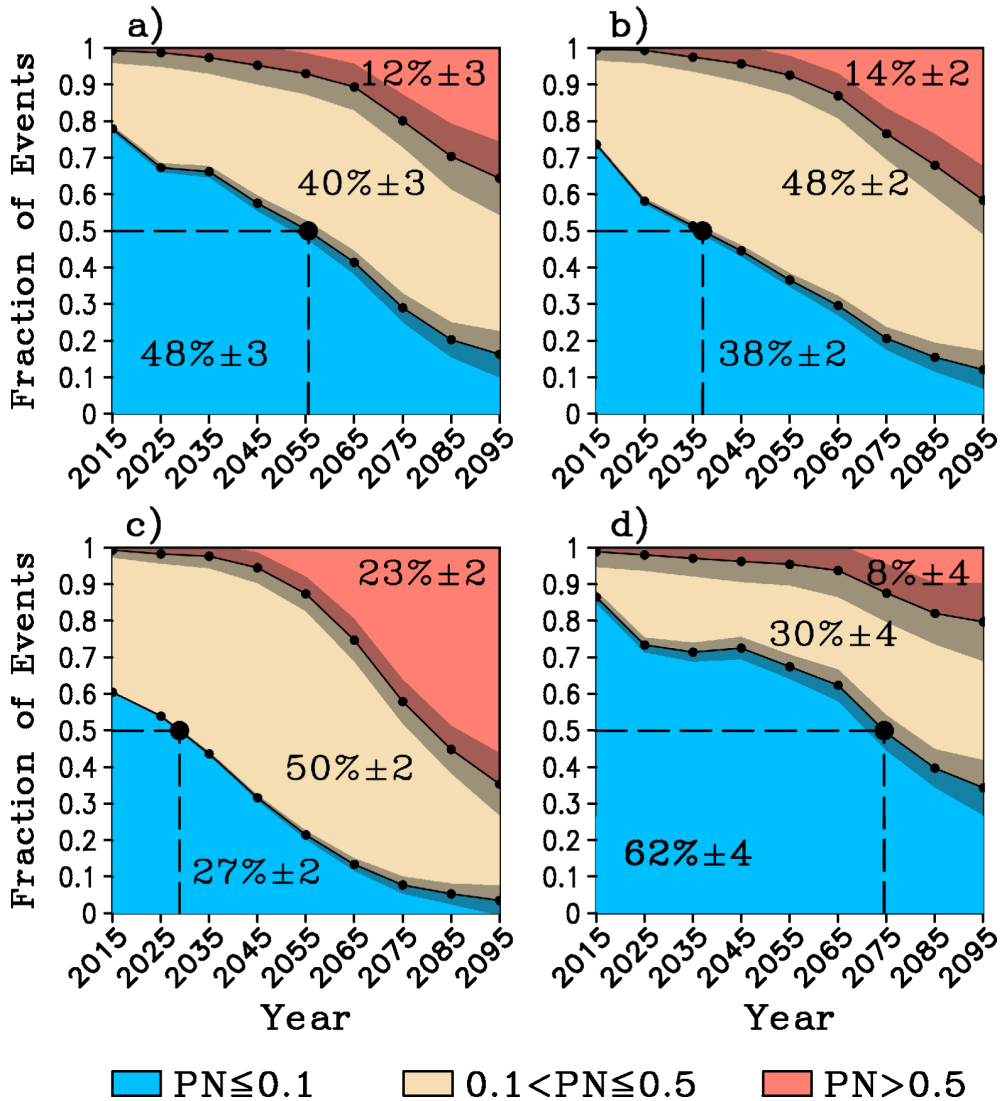


**Figure 4.** Evolution of the probability of necessary causation (PN) of heat wave events into the 21<sup>st</sup> Century for the a) Northern Plains, b) Great Lakes, c) Western, and d) Southern Plains regions. PN values less than 0.1 (blue) indicate anthropogenic climate change (ACC) is not a necessary condition for most heat extremes (e.g., internal variability dominates ACC effects). PN values greater than 0.5 (red) suggest ACC is a necessary condition for more than half of the temperature extremes (e.g., ACC dominates). The black circle at the intersection of the dashed lines denotes when ACC becomes a major contributor to heat extremes (e.g., a measure of the time of emergence). The percentage values indicate the fraction of heat extremes attributed to each category. The plus/minus value and the gray shading indicates 95% confidence interval by randomly selecting 20 ensemble members 500 times and repeating the analysis.

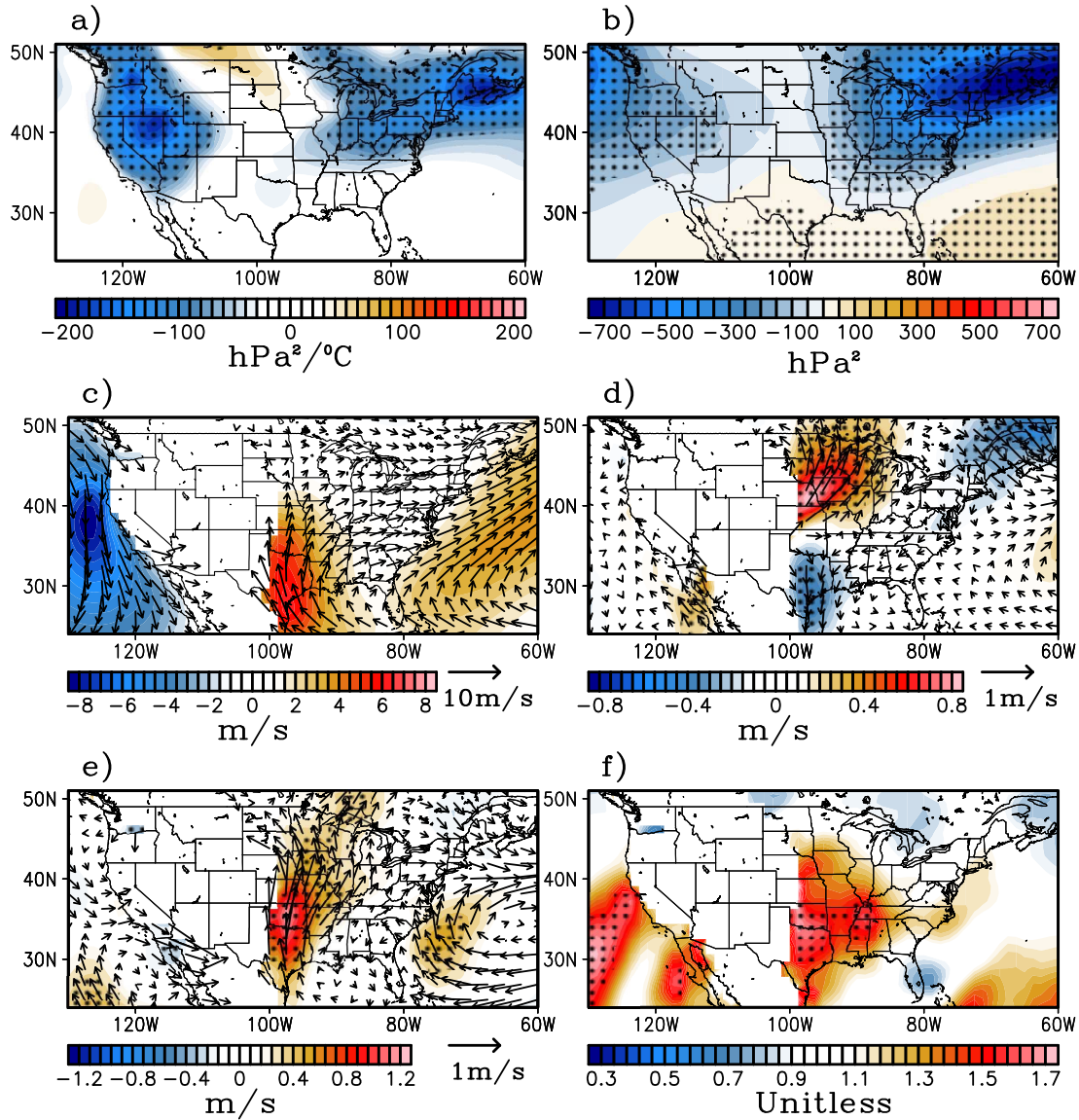


**Figure 5.** a) Regression of atmospheric transient eddies (storms) and 2-m air temperature for June-July-August (JJA) in units of  $\text{hPa}^2/\text{°C}$ . b) Projected changes (e.g., 21<sup>st</sup> minus 20<sup>th</sup> Century) of JJA atmospheric transient eddies [ $\text{hPa}^2$ ]. Transient eddies or storminess is defined as the square of the departure from the monthly mean of daily mean geopotential height at 500hPa. c) CMIP5 ensemble mean 925hPa wind (vector) and meridional wind component (color) during June-July-August (JJA) from the historical period (i.e., 1920-2005). d) Same as c) but showing the composite during both Northern and Southern Great Plains heat waves from the historical period. e) Same as c) but for the projected mean circulation changes (e.g., 21<sup>st</sup> minus 20<sup>th</sup> Century) in JJA 925hPa winds. f) Variance ratio of 21<sup>st</sup> to 20<sup>th</sup> Century JJA 925hPa meridional wind. Stipples in panels a), b), c) and d) indicate 95% confidence level based on a Student-T test. Stipples in panel f) indicate 95% confidence level based on an F-test. Regions where surface pressure is less than 925hPa are masked out.